IASS 2020/21 SURREY 7
International Conference on Spatial Structures 2020/21

Proceedings of the IASS Annual Symposium 2020/21 and the 7th International Conference on Spatial Structures
Inspiring the Next Generation
23 – 27 August 2021, Guilford, UK
S.A. Behnejad, G.A.R. Parke and O.A. Samavati (eds.)

Generating developable and rigidly foldable origami surfaces with arbitrary Gaussian curvatures

Sree Chandana MADABHUSHI[a], Kishore Sreekumar SHENOY[b], Phanisri Pradeep PRATAPA*

[a b] *Dept. of Civil Engineering, Indian Institute of Technology Madras, Chennai 600036, India
ppratapa@civil.iitm.ac.in

Abstract

Origami-based deployable surfaces that are developable as well as rigidly foldable are of interest in various architectural and engineering applications. Such structures have been researched in recent years using inverse design techniques based on optimization by formulating an under-constrained equation system that governs the design solution. We present an alternative framework that involves directly solving an over-constrained system of equations that dictate the design of generalized Miura-ori surfaces that conform to target surfaces of zero, positive, and negative Gaussian curvatures. The constraint equations involve imposing the developability of vertices, planarity of origami panels, and local flat-foldability of vertices. We discuss the accuracy of design solutions both with and without the imposition of flat-foldability, that is critical for strain free deformation of the origami system. The results highlight the feasibility of obtaining practically usable target origami surfaces that are developable and rigidly foldable, using a least-squares-based solution of heavily over-constrained system of equations.

Keywords: origami, Miura-ori, deployable surfaces, rigidly foldable, developable, inverse-origami, transformable structures.

1. Introduction

Origami allows the creation of folded structures that can take any target shape. These structures can incorporate kinematics by controlling the angles of the origami folds, which opens new possibilities to create "living" structures. Our work is concerned about designing foldable surfaces of arbitrary Gaussian curvature based on origami. Specifically, we are interested in generating variants of the Miura-ori pattern (Miura and Lang [9]) that are both developable and rigid foldable, and will fit a target surface at a partially folded state. Developability is the ability of the pattern to fold from a flat sheet, whereas rigid foldability ensures that the shape changing of the system primarily happens through folding and that all the panels remain undeformed.

Manipulating the crease geometry of the origami patterns to form different surfaces is a fundamental idea explored by many researchers. For example, Tachi [14,15] presented frameworks, where one could perturb the vertices of a standard Miura-ori pattern to distort the origami structure into complex shapes. Schenk and Guest [13], Wei *et al*. [17], Nassar *et al*. [10], Pratapa *et al*. [11], explored the possible shapes particular origami patterns can fold into. However, inverse design of origami patterns to fit a desired surface is relatively less studied and is still an area of active research. Recently, researchers have employed optimization-based frameworks to design generalized Miura-ori structures to fit target surfaces, while choosing some of the vertex coordinates as design variables (Dudte *et al*. [1], Feng *et al*. [2], Hu *et al*. [6]). In these works, the developability, planarity of the origami panels, and local vertex flat-foldability conditions are enforced to be satisfied in the obtained design solutions. In addition to this, it is required that the geometry of a partially folded state of the origami structure should conform to a target surface in some sense. In general, these requirements make the system over-constrained,

especially when hard constraints are imposed on the location of vertices. To enable the use of optimization, most of the vertices are allowed to move freely, while minimizing a suitably defined objective function, to design the origami structure that fits a target surface.

As an alternative to the optimization-based approaches, in this paper, we present and investigate a procedure to find the design solutions by directly solving the over-constrained system of equations using a least-squares-based approach. The motivation for this is twofold. Firstly, using an optimization-based approach needs a definition of objective function that introduces some ambiguity between various choices, and also needs the system to be under-constrained, restricting the imposition of hard constraints. Secondly, an approximate solution using least-squares type methods may be of interest in large length-scale practical applications, where the non-zero residuals in the equations can be accommodated within working tolerances of the origami structure. Therefore, it is worth exploring the feasibility of obtaining solutions using the over-constrained equation framework. By leveraging the over-constrained nature of the framework, we investigate possible solutions by imposing hard constraints, i.e., we try to enforce the conformation of all the top vertices of the pattern to a target surface. We then look at relaxation strategies to control the accuracy of the solutions obtained. We also introduce limits on the maximum perturbations that the free vertices can undergo.

This paper is organized as follows. In Section 2, we describe the geometry of the Miura-ori structure. In Section 3, we explain the problem set up and solution procedure that will be adopted. After that, in Section 4, we present the results when the flat-foldability conditions are not applied, for three target surfaces with zero, positive, and negative Gaussian curvatures. We briefly discuss the practical relevance of such design solutions. Finally, in Section 5, we discuss the imposition of local flat-foldability, which makes the equations more over-constrained and solutions less accurate. To overcome the issue, we present some relaxation strategies that can improve the accuracy of the solutions.

2. Geometry of standard and generalized Miura-ori

The standard Miura-ori tessellation is a simple deployable origami structure that can be folded up from a flat sheet of material. Its crease pattern, shown in Fig. 1(a), comprises a set of parallelogram shaped panels that are repeated regularly. The corners of the panels form degree-4 vertices where the mountain and valley creases intersect. It can be rigidly folded to any state up to the flat folded one, without inducing any mechanical strain in the panels. At any partially (or intermediate) folded state, all the vertices lie on either of the two imaginary parallel surfaces at the top or the bottom of the structure (see Fig. 1(b)).

A standard Miura-ori pattern has only one type of vertex, which is a degree-4 vertex with three mountains and one valley or vice versa. The pattern can be obtained by tessellating a single unit cell that comprises four parallelogram shaped panels and one degree-4 vertex formed by their intersection. The geometry of the pattern can be described in a Cartesian system by assigning coordinates to all the vertices. For a standard Miura-ori, a single panel angle uniquely describes the angles of all the parallelograms in the tessellation. Further geometric description of the panels is given by the edge lengths.

The generalized Miura-ori structure can be obtained by perturbing the position of the vertices in the crease pattern of standard Miura-ori (Fig. 1(a)), while ensuring that the pattern is still developable, flat-foldable, and all the panels remain as planar quadrilaterals. For this reason, it is also referred to as a quadrilateral mesh origami (Tachi [14]). The last requirement on the planarity and the quadrilateral nature of the panels ensures the single degree of freedom deployable nature of the resulting structure if it can undergo rigid-folding. Unlike standard Miura-ori, the generalized version need not be a tessellation, and its panels need not be parallelograms. However, the mountain-valley assignment of the

creases is left unchanged. Each degree-4 vertex of the generalized Miura-ori can be identified with four different panel angles.

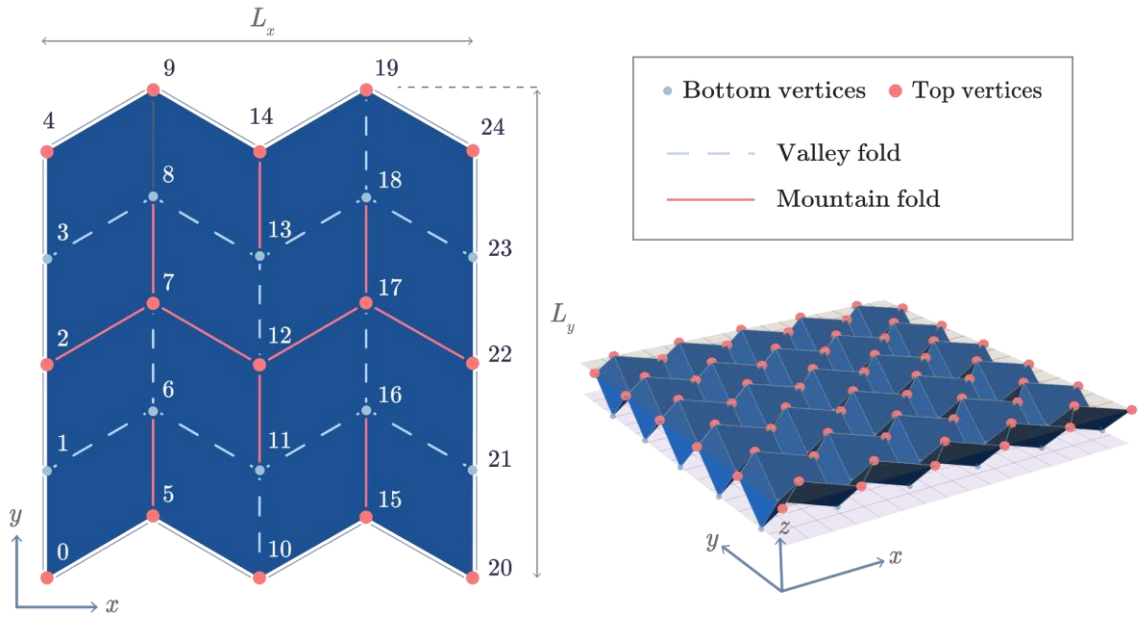

Figure 1: Left: 2x2 standard Miura-ori tessellation with vertices indexed starting from 0 at bottom left. Right: Partially folded state of a 5x5 tessellation.

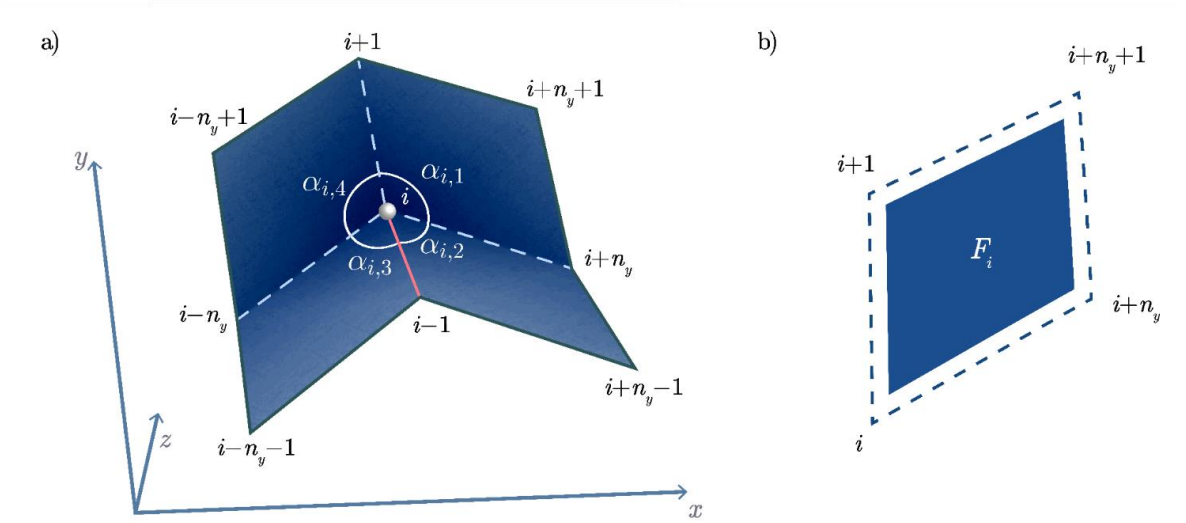

Figure 2: a) A Miura-ori unit cell with panel angles around the central vertex and a generalised indexing of vertices. b) A face (panel) F_i of the pattern indexed by the vertex of lowest index.

3. Problem setup

In this study, we are interested in seeking the spatial perturbations of all the vertices of a standard Miura-ori crease pattern, that will lead to a partially folded configuration of the origami system, which can approximate surfaces of desired Gaussian curvature. Instead of starting from a crease pattern and then perturbing the vertices, we start from an initial configuration of vertices identified based on the target

surface, and then impose various constraints that are necessary to obtain a generalized Miura-ori. In this section, we discuss the details of the notation adopted, the constraints that are considered, and the solution procedure employed.

3.1. Notation

The size of the Miura-ori pattern is represented in terms of the number of unit cells as $N_x \times N_y$ with n_x number of vertices along the x-direction and n_y number of vertices along the y-direction. They are related as,

$$n_x = 2N_x + 1, n_y = 2N_y + 1. \tag{1}$$

Using the order of vertex indexing as shown in Fig. 1(a), and setting the origin at the vertex 0, the Cartesian coordinates of a vertex i are defined by,

$$v_i \ = [x_i, y_i, z_i]. \tag{2}$$

The four panel angles associated with vertex i are denoted by $\alpha_{i,1}, \alpha_{i,2}, \alpha_{i,3}$ and $\alpha_{i,4}$ as shown in Fig. 2(a), and can be calculated using appropriate dot products. For example,

$$\alpha_{i,1} = \arccos\left[\frac{\left(\vec{v}_{i+1} - \vec{v}_i\right) \cdot \left(\vec{v}_{i+n_y} - \vec{v}_i\right)}{\vec{v}_{i+1} - \vec{v}_i \left|\vec{v}_{i+n_y} - \vec{v}_i\right|}\right]. \tag{3}$$

A face (also referred to as facet or a panel) is represented by the set of its four corner vertices. Each face is indexed based on the index of the left-bottom vertex of the face, as shown in Fig. 2(b). So, a face F_i is defined by the set of vertices $\{i, i+1, 1+n_y+1, i+n_y\}$.

3.2. Developability (Dev) and facet-planarity (PoF) constraints

To ensure developability (Dev), angles at each interior vertex i should satisfy the equation,

$$\mathrm{Dev}_i = \sum_{j=1}^{4} \alpha_{i,j} - 2\pi = 0. \tag{4}$$

The planarity of facets (PoF) constraints make sure that the final structure has panels which are all planar quadrilaterals. This is a necessary condition to ensure that the structure is deployable through a single degree of freedom kinematics. This constraint is mathematically represented for each face F_i by the equation,

$$\mathrm{PoF}_i = \frac{\left(\vec{v}_{i+1} - \vec{v}_i\right)}{\vec{v}_{i+1} - \vec{v}_i} \times \frac{\left(\vec{v}_{i+n_y} - \vec{v}_i\right)}{\left|\vec{v}_{i+n_y} - \vec{v}_i\right|} \cdot \frac{\left(\vec{v}_{i+n_y+1} - \vec{v}_i\right)}{\left|\vec{v}_{i+n_y+1} - \vec{v}_i\right|} = 0. \tag{5}$$

3.3. Flat-foldability (FF) constraints

The Dev and PoF conditions mentioned above allow us to get generalized Miura-ori-like solutions. But they are not sufficient to ensure strain-free rigid folding of the obtained origami structure. In order to achieve this, we also need to impose local flat-foldability (FF) constraint at each interior vertex. Using Kawasaki's theorem (Lang [7]), these constraints at each interior vertex i are given by,

$$\mathrm{FF}_i = 2(\alpha_{i,1} + \alpha_{i,3} - \pi) = 0. \tag{6}$$

In cases where we do not enforce FF constraints, we calculate the flat-foldability residuals as FF_i at each interior vertex of the final geometry.

3.4. Target surface constraints

In order to constrain the top vertices to the target surface, we update the z-coordinates of each top vertex i, at each iteration as follows, $z_i = S[x_i, y_i]$, where S represents the z-coordinate of the target surface function that is of interest. This constraint still allows for the top vertices to slide on the target surface.

3.5. Design variables, initial guess, and perturbation bounds (Tol)

The set of variables is the x, y and z-coordinates of all vertices, along with the "thickness" d of the structure. This thickness variable is the z-offset between the top surface and the averaged bottom surface. Since, the top vertices are constrained to stay on the target surface, the z-coordinates of the top vertices are not free variables. Therefore, the design variable set reduces to

$$\text{variables} = \left[\ x_i, y_i, z_{i\ \ bottom},\ \ x_i, y_{i\ \ top}, d\right].$$

The initial guess pattern of the origami structure is obtained by projecting the standard Miura-ori crease pattern onto the target surface, as shown in Fig. 3. The z-coordinates of the top vertices are obtained directly from the target surface, whereas, those of the bottom vertices are obtained from an offset of the target surface by thickness d_0 along the z-direction. We denote the x, y-coordinates of the vertices in the initial pattern as $x_{i,0}$, $y_{i,0}$ respectively.

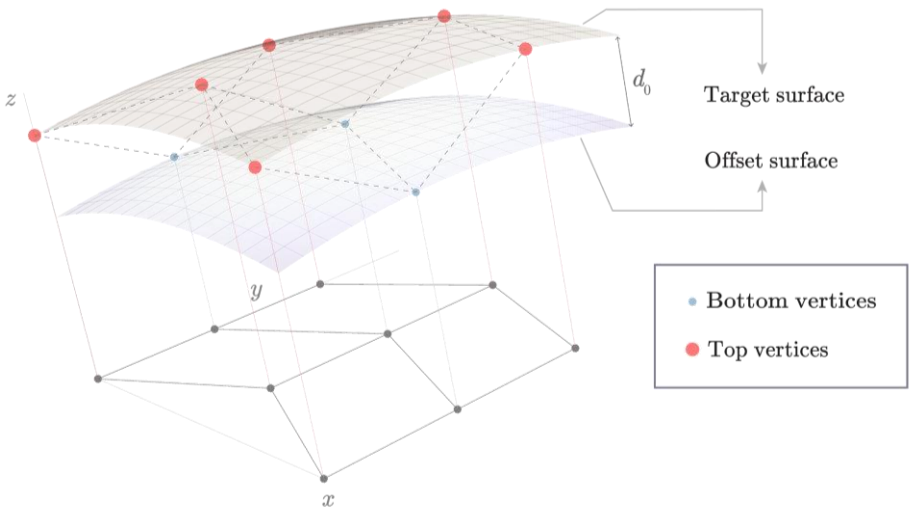

Figure 3: Obtaining the initial guess by projection of the 2D crease pattern. The broken lines represent edges of the initial guess structure.

To limit the deviations from the initial pattern so that the solution is Miura-like, some of the variables are loosely constrained as follows. The x and y-coordinates of the top vertices are bounded as,

$$x_i \in [x_{i,0} - t_{xy}, x_{i,0} + t_{xy}] \text{ and } y_i \in [y_{i,0} - t_{xy}, y_{i,0} + t_{xy}].$$

The z-coordinates of the bottom vertices are allowed to deviate within a bound (t_z) from the bottom surface (determined by d) as follows,

$$z_i \in [z_{i,0} - t_z, z_{i,0} + t_z], \text{ where } z_{i,0} = S[x_i, y_i] - d.$$

Also, the z-offset (d) between the top and bottom surfaces is bound as follows,

$$d \in [d_0 - t_d, d_0 + t_d].$$

These bounds are reformulated as constraint equations (Tol) in terms of continuous differentiable piecewise functions (see Fig. 4). For each bounding tolerance of the form

$$p \in [p_0 - t_p, p_0 + t_p],$$

we impose an equation,

$$\mathrm{Tol}_p = 0, \tag{7}$$

$$\text{where } \mathrm{Tol}_p = \begin{cases} 0, & p \in [p_0 - t_p, p_0 + t_p] \\ (|p_0 - p| - t_p)^2, & \text{otherwise} \end{cases}.$$

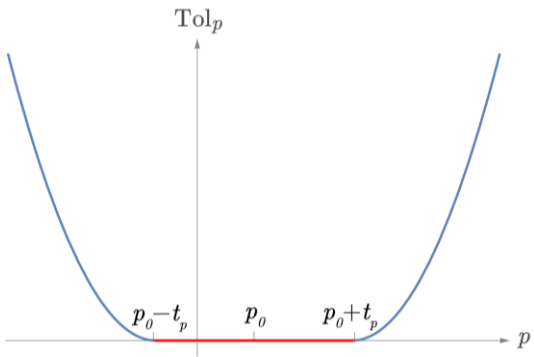

Figure 4: The continuous differentiable piecewise function that represents the Tol equations.

3.6. Solution procedure

The total number of free variables available for the design of the origami structure is $3n_x n_y - (N_y + 1)n_x + 1$. We shall first consider only the equations that are to be satisfied by these variables without imposing the local flat-foldability of the vertices, i.e. Dev, PoF, and Tol. These add up to a total of $n_x - 2\ (n_y - 2) + n_x - 1\ (n_y - 1) + 2(N_y + 1)n_x + N_y n_x + 1$. For a simple case when $N_x = N_y = N$, the total number of variables and equations are $10N^2 + 9N + 3$ and $14N^2 + 3N + 4$, respectively.

The number of equations in excess of the variables increases with N and is given by $4N^2 - 6N + 1$. Therefore, the design problem is set up as an over-constrained system of nonlinear equations that need to be solved. For example, when $N = 5$, there are 369 equations and only 298 free variables. Note however, that the Tol equations corresponding to the bounds on the perturbation of the vertices are relatively loose constraints that are rarely violated when good enough solutions exist for the system of equations. Moreover, violation of the Tol equations does not compromise the necessary design

constraints like developability and rigid foldability, as long as no crossover/intersection/merging of the vertices occurs. When the flat-foldability (FF) equations are also included in the framework, the excess of equations increase by $2N-1$ [2].

We solve this over-constrained system of nonlinear equations in a least-squares sense using a modified Levenberg-Marquardt algorithm available through the `lm` method in the SciPy package of Python ([5], Virtanen *et al.* [16]). We choose to design origami structures having 5×5 cells, with the dimensions of the initial developed geometry as $L_x = L_y = 75$ units. The perturbation bounds are chosen as $t_{xy} = 7.5$ units, and $t_z = t_d = 5.625$ units. The initial z-offset is chosen as $d_0 = 11.25$ units.

4. Results with finite flat-foldability residuals

In this section, we discuss the solutions obtained when the local flat-foldability (FF) constraints (Eq. (6)) are not imposed. This provides us insight on the ease of obtaining the design solutions in a relatively less constrained space. The absence of FF conditions prevents the origami structure from undergoing strain free folding. The strain energy associated with such deformations can be correlated with the flat-foldability residuals defined in Sec 3.3 (Dudte *et al.* [1]). Although such a behavior seems undesirable, it may not be avoidable in certain applications. For example, architectural and civil engineering applications (Filipov *et al.* [3], Reis *et al.* [12]) involving large deployable structures could entail panels with high self-weight which will induce mechanical strains in the origami structure. Comparison of the strains induced (using origami simulation tools like Liu *et al.* [8], and Ghassaei *et al.* [4]) due to the FF residuals in relation to the strains induced due to the structural loads could be investigated in the future.

The developability (Dev) as well as the planarity of facets (PoF) constraints are solved for, while imposing the bounds on the perturbation of vertices through tolerance equations (Tol). Therefore, any successful solution from the solver will still have developable vertices and planar quadrilateral panels in the partially folded state representing the target surface. We consider three target surfaces: (1) parabolic arch, (2) paraboloid (dome), and (3) hyperbolic paraboloid (saddle), to represent zero, positive, and negative Gaussian curvatures, respectively. The design solutions obtained by solving the equations without imposing FF constraints are presented in Fig. 5. In the figure, the values of the parameter k indicate the maximum curvature along the x-direction for which the solver could successfully converge. In Table 1, we have provided the residuals of the equations corresponding to the design solutions obtained.

Table 1: Equation residuals for design solutions when FF constraints are not imposed. The root mean square values for each set of equations are provided with the absolute maximum values indicated in the parentheses. The units correspond to those adopted in the respective equations. Angles are measured in radians and lengths are measured in non-dimensional units.

	Dev	PoF	FF	Tol_{xy}	Tol_z	Tol_d
Arch	1.08e-15 (3.55e-15)	1.04e-12 (4.98e-12)	2.19e-02 (4.87e-02)	0.0 (0.0)	4.21e-07 (2.15e-06)	0.0 (0.0)
Dome	5.32e-15 (2.49e-14)	9.60e-13 (3.77e-12)	1.96e-01 (6.68e-01)	0.0 (0.0)	2.08e-06 (6.36e-06)	0.0 (0.0)
Saddle	1.17e-15 (4.44e-15)	8.30e-13 (2.71e-12)	6.73e-02 (1.56e-01)	0.0 (0.0)	7.77e-07 (2.38e-06)	0.0 (0.0)

It can be seen from Table 1 that very good accuracy could be obtained across all the imposed conditions (Dev, PoF, and Tol). Despite being a seemingly over-constrained system of equations, the fully converged solutions indicate that the perturbation bounds on the vertices (Tol) act as guidelines in finding the origami structures depicting the targeted surfaces. We have found that very few perturbation bounds have been violated, and even in those cases, no crossover or merging of vertices has occurred. So, out of the 187 Tol equations, most of them are easily satisfied making the system of equations act as if they were under-constrained, and therefore resulted in achieving solutions with good accuracy. Table 1 also indicates the FF residuals calculated from the final solutions obtained. We found that the FF residuals are less than about 5°, on average across the vertices, for the arch and the saddle, with a few vertices showing significant residual as high as about 10°. However, the solution obtained for the dome indicates that it has much higher FF residuals across vertices in general, reaching as high as 30° at certain vertices.

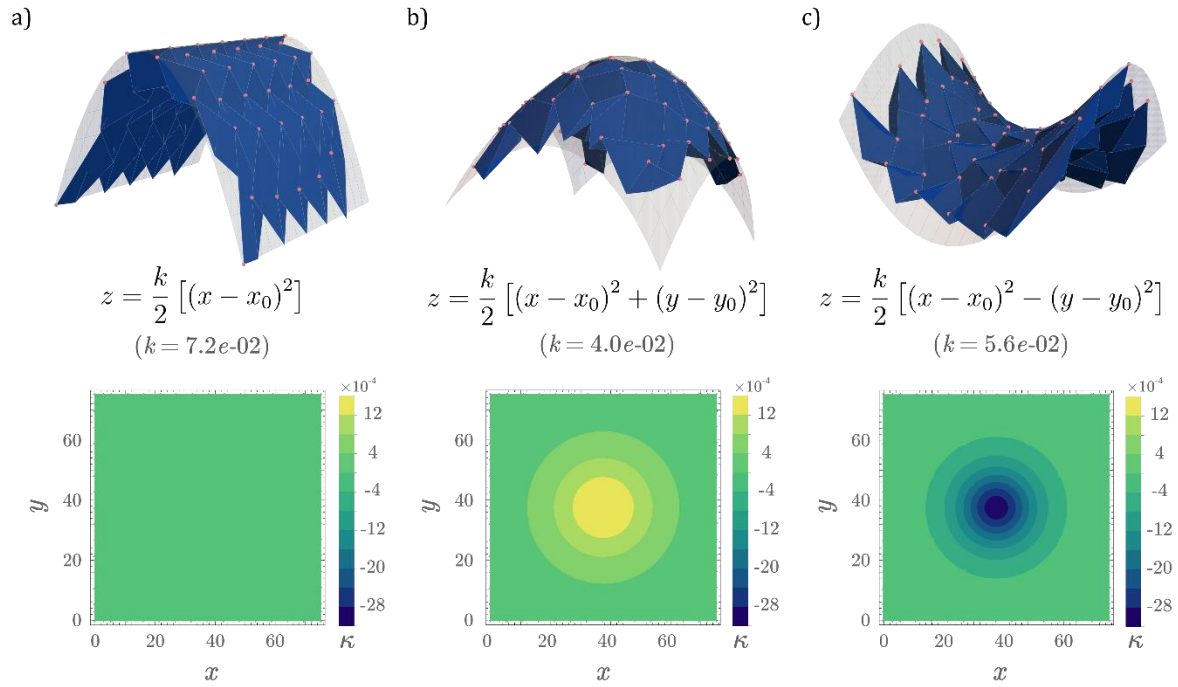

Figure 5: Top row: Visualization of the design solutions obtained when local flat-foldability is not imposed. The target surface equations for each case are indicated below the visualizations. a), b), and c) correspond to the zero (arch), positive (dome), and negative (saddle) Gaussian curvature cases, respectively. Bottom row: Color contours of the Gaussian curvatures (κ) of the target surfaces in the domain.

5. Inclusion of flat-foldability constraints

It was shown previously by researchers that if a valid partially folded state of the origami structure exists, and the local flat-foldability condition holds at all interior vertices, then the structure is rigid-foldable (Dudte *et al.* [1]). If the developability (Dev) and planarity of facets (PoF) constraints are expected to be satisfied, the partially folded state corresponding to the desired target surface is a valid state. Therefore, additional satisfaction of the FF equations ensures strain free folding of the origami structure. In this section, we will study the ease of solving the constraint equations by incorporating local flat-foldability (FF) conditions (Eq. (6)), in addition to the Dev, PoF, and Tol equations considered in the previous section. We choose the same target surfaces and corresponding k values

discussed previously in Fig. 5. Specifically, we first show that imposing FF equations makes the system heavily over-constrained and does not lead to satisfactory solutions in general. To overcome this problem, we discuss two relaxation strategies, namely (1) Patch size reduction, and (2) Releasing some top vertices, to potentially find more accurate solutions.

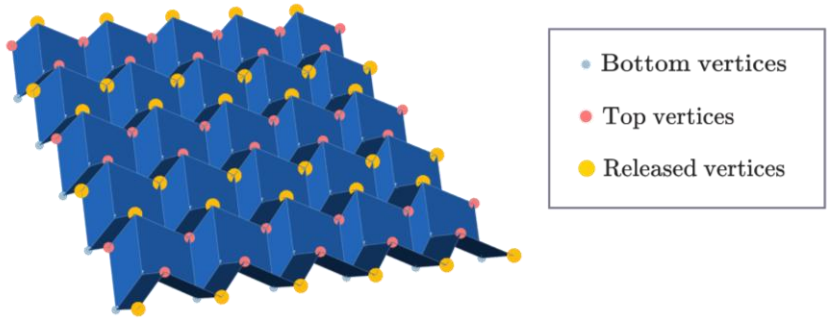

Figure 6: Top vertices that are completely released to behave as free variables in the relaxation strategy 2.

In the first strategy, we reduce the domain size on which the target surface is defined. It is straightforward to fit the Miura-ori pattern to a flat surface. Therefore, the idea behind this relaxation strategy is to bring the target surface closer to a flat surface. For any surface equation given in Fig. 5, the deviation of vertices from a tangent plane at the midpoint of the target surface increases with the increase in domain (or patch) size (L_x or L_y), which makes the problem harder to solve. Hence, in this strategy, we try to fit the generalized Miura-ori on a target surface defined on a reduced patch size, that requires smaller deviations of the vertices from a flat surface. In the second strategy, we release some of the top vertices that were all originally constrained to slide on the target surface. Specifically, we release one vertex per unit cell in an alternating fashion as shown in Fig. 6. The motivation behind this strategy is that, releasing some vertices gives more free variables to the equation system that must be solved, making it more amenable.

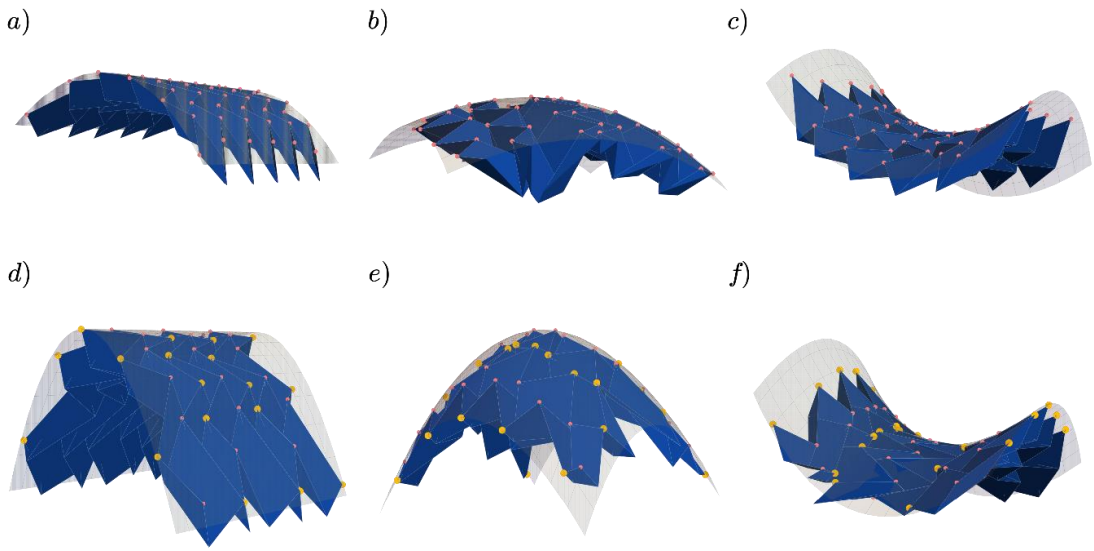

Figure 7: Design solutions obtained by employing relaxation strategies 1 (a-c), and 2 (d-f). In a-c, the patch size is $75/2$, and all the top vertices lie on the target surface. In d-f, patch size is 75, and the top vertices highlighted with larger (yellow) dots may not lie on the target surface.

Table 2: Influence of relaxation strategies on the accuracy of solutions obtained for the three target surfaces. The root mean square values of the residuals calculated for each set of equations are provided below, with the absolute maximum values indicated in the parentheses.

Arch	Dev	PoF	FF	Tol_{xy}	Tol_z	Tol_d
No relaxation	1.22e-08 (4.26e-08)	8.40e-09 (2.49e-08)	1.22e-08 (4.30e-08)	2.47e-06 (2.47e-05)	0.0 (0.0)	0.0 (0.0)
Relaxation-1 Patch Size 75/2	3.19e-10 (1.00e-09)	3.41e-10 (1.32e-09)	3.17e-10 (1.03e-09)	0.0 (0.0)	0.0 (0.0)	0.0 (0.0)
Relaxation-2 Released some vertices	7.90e-16 (2.66e-15)	1.33e-16 (5.80e-16)	8.99e-16 (3.55e-15)	1.65e+00 (1.09e+01)	0.0 (0.0)	0.0 (0.0)

Dome	Dev	PoF	FF	Tol_{xy}	Tol_z	Tol_d
No relaxation	1.22e-04 (4.01e-04)	3.27e-04 (1.47e-03)	1.20e-04 (3.96e-04)	2.14e-03 (9.00e-03)	1.50e-03 (8.30e-03)	0.0 (0.0)
Relaxation-1 Patch Size 75/2	8.20e-16 (1.78e-15)	1.98e-16 (7.23e-16)	9.26e-16 (2.66e-15)	5.18e-08 (2.95e-07)	1.52e-08 (1.12e-07)	0.0 (0.0)
Relaxation-2 Released some vertices	1.82e-10 (1.64e-09)	2.98e-08 (2.98e-07)	1.74e-10 (1.56e-09)	4.51e-01 (3.76e+00)	2.23e-01 (1.18e+00)	0.0 (0.0)

Saddle	Dev	PoF	FF	Tol_{xy}	Tol_z	Tol_d
No relaxation	7.90e-05 (2.80e-04)	1.74e-04 (8.00e-04)	7.87e-05 (2.97e-04)	1.17e-03 (5.93e-03)	1.21e-03 (4.68e-03)	6.13e-03 (6.13e-03)
Relaxation-1 Patch Size 75/2	8.72e-16 (1.78e-15)	2.50e-16 (1.45e-15)	7.83e-16 (1.78e-15)	1.31e-08 (1.32e-07)	0.0 (0.0)	0.0 (0.0)
Relaxation-2 Released some vertices	2.81e-09 (2.28e-08)	5.48e-08 (5.38e-07)	1.54e-09 (1.36e-08)	2.77e-01 (3.18e+00)	1.08e+00 (4.24e+00)	0.0 (0.0)

We present the results obtained by employing the above-mentioned strategies, in Table 2, and Fig. 7. Firstly, it can be noted that for all three examples (arch, dome, and saddle), when no relaxation strategy was used, although the FF residuals are lower than that obtained in Sec 4 (see Table 1), the other

equations are not solved accurately enough. By employing the relaxation strategies independently of one another, we find that the accuracy of the solutions obtained can be improved significantly. This is possible due to the trade-off on the size of target surface in the strategy-1, and deviation of some top vertices from the target surface when using the strategy-2.

5. Conclusion

In this paper, we have presented a framework to design developable and rigidly foldable generalized Miura-ori patterns that can conform to a target surface at some partially folded state. We have considered three target surfaces with zero (arch), positive (dome), and negative (saddle) Gaussian curvatures. Unlike the previous studies that focused on setting up an under-constrained system of equations and adapting an optimization framework to design the patterns, we considered over-constrained systems of equations and directly solved them using a least-squares-based approach. In addition to the required mathematical conditions on developability, facet-planarity, and flat-foldability, we also imposed conditions on the maximum amount of perturbation that each vertex can undergo in order to satisfy the equations.

We have first shown that the equations can be solved with reasonable accuracy when the flat-foldability conditions are not imposed. We then discussed the difficulty in accurately solving the equations when the flat-foldability conditions are imposed and presented relaxation strategies that lead to more accurate solutions. Specifically, we have shown that the accuracy of solutions obtained by directly solving the over-constrained system can be controlled by either reducing the patch size of the target surface, or by removing the restrictions on some of the top vertices that were constrained to slide on the target surface.

In summary, the presented framework offers an alternative procedure for inverse design of origami patterns conforming to target surfaces. Future work could involve studying the energetic feasibility of folding the origami designs obtained here, especially when the flat-foldability residuals are not very small. The applicability of the current framework to study more complicated surfaces could also be investigated.

Acknowledgements

Phanisri Pradeep Pratapa acknowledges the financial support from the seed grant provided by Indian Institute of Technology Madras, and the support from the Science & Engineering Research Board (SERB) of the Department of Science & Technology, Government of India, through award SRG/2019/000999.

References

[1] Dudte, L., Vouga, E., Tachi, T. and Mahadevan, L., 2016. Programming curvature using origami tessellations. *Nature Materials*, 15(5), pp.583-588.

[2] Feng, F., Dang, X., James, R. and Plucinsky, P., 2020. The designs and deformations of rigidly and flat-foldable quadrilateral mesh origami. *Journal of the Mechanics and Physics of Solids*, 142, p.104018.

[3] Filipov, E., Tachi, T. and Paulino, G., 2015. Origami tubes assembled into stiff, yet reconfigurable structures and metamaterials. *Proceedings of the National Academy of Sciences*, 112(40), pp.12321-12326.

[4] Ghassaei, A., Demaine, E. and Gershenfeld, N., 2021. Fast, Interactive Origami Simulation using GPU Computation. *Origami 7*, 4, pp.1151-1166.

[5] https://docs.scipy.org/doc/scipy/reference/optimize.root-lm.html#optimize-root-lm

[6] Hu, Y., Zhou, Y. and Liang, H., 2021. Constructing Rigid-Foldable Generalized Miura-Ori Tessellations for Curved Surfaces. *Journal of Mechanisms and Robotics*, 13(1).

[7] Lang, R.J., 2017. *Twists, tilings, and tessellations: Mathematical methods for geometric origami*. CRC Press.

[8] Liu, K. and Paulino, G.H., 2017. Nonlinear mechanics of non-rigid origami: an efficient computational approach. *Proceedings of the Royal Society A: Mathematical, Physical and Engineering Sciences*, 473(2206), p.20170348.

[9] Miura, K. and Lang, R.J., 2009. The science of Miura-ori: A review. *Origami 4*, pp.87-99.

[10] Nassar, H., Lebée, A. and Monasse, L., 2017. Curvature, metric and parametrization of origami tessellations: theory and application to the eggbox pattern. *Proceedings of the Royal Society A: Mathematical, Physical and Engineering Sciences*, 473(2197), p.20160705.

[11] Pratapa, P., Liu, K. and Paulino, G., 2019. Geometric Mechanics of Origami Patterns Exhibiting Poisson's Ratio Switch by Breaking Mountain and Valley Assignment. *Physical Review Letters*, 122(15), p.155501.

[12] Reis, P., López Jiménez, F. and Marthelot, J., 2015. Transforming architectures inspired by origami. *Proceedings of the National Academy of Sciences*, 112(40), pp.12234-12235.

[13] Schenk, M. and Guest, S., 2013. Geometry of Miura-folded metamaterials. *Proceedings of the National Academy of Sciences*, 110(9), pp.3276-3281.

[14] Tachi, T., 2009. Generalization of Rigid Foldable Quadrilateral Mesh Origami. *Journal of the International Association for Shell and Spatial Structures*, 50(3), pp.173-179.

[15] Tachi, T., 2010. Freeform Variations of Origami. *Freeform Variations of Origami*, 14(2), pp.203-215.

[16] Virtanen, P., Gommers, R., Oliphant, T., Haberland, M., Reddy, T., Cournapeau, D., Burovski, E., Peterson, P., Weckesser, W., Bright, J., van der Walt, S., Brett, M., Wilson, J., Millman, K., Mayorov, N., Nelson, A., Jones, E., Kern, R., Larson, E., Carey, C., Polat, İ., Feng, Y., Moore, E., VanderPlas, J., Laxalde, D., Perktold, J., Cimrman, R., Henriksen, I., Quintero, E., Harris, C., Archibald, A., Ribeiro, A., Pedregosa, F. and van Mulbregt, P., 2020. SciPy 1.0: fundamental algorithms for scientific computing in Python. *Nature Methods*, 17(3), pp.261-272.

[17] Wei, Z.Y., Guo, Z.V., Dudte, L., Liang, H.Y. and Mahadevan, L., 2013. Geometric mechanics of periodic pleated origami. *Physical Review Letters*, 110(21), p.215501.